Soft Matter

PAPER

View Article Online
View Journal | View Issue

Cite this: *Soft Matter*, 2015, 11, 7367

Synergistic assembly of nanoparticles in smectic liquid crystals†

Apiradee Honglawan,[a] Dae Seok Kim,[b] Daniel A. Beller,‡[c] Dong Ki Yoon,[b] Mohamed A. Gharbi,[acd] Kathleen J. Stebe,[a] Randall D. Kamien[c] and Shu Yang*[ad]

Received 12th June 2015,
Accepted 10th August 2015

DOI: 10.1039/c5sm01458a

www.rsc.org/softmatter

We report synergistic co-assembly between smectic A liquid crystal (SmA LC) and planar anchoring fluorosilane functionalized silica (F-SiO_2) nanoparticles (NPs). Both scanning electron microscope (SEM) images and grazing incidence X-ray diffraction (GIXD) patterns show that when cooled from the isotropic phase to SmA phase, F-SiO_2 NPs (100–500 nm in diameter) migrate from the bottom to the top of the LC film through the central cusp defects of toric focal conic domains (TFCDs). When the NPs form a monolayer on top, replacing the LC/air interface, vertically aligned SmA layers are formed between the top and bottom planar surfaces. When F-SiO_2 NP diameter is small (<500 nm), we observe a weak-anchoring regime, where NPs do not cause appreciable layer curvature and NP migration is driven by surface energy. When F-SiO_2 particle diameter > 500 nm, strong distortions occur in the smectic layers, and the particle is found suspended at the TFCD defect core. The knowledge of the intermediate states of the NP/LC hybrid structures will provide valuable insights to assemble functional nanomaterials such as quantum dots and metallic NPs in an anisotropic medium, and take advantage of their collective assembly behaviors to create more complex and dynamic structures.

Introduction

As building blocks, nanoparticles (NPs) offer a dizzying array of size, shape, chemistry, and surface functionality with unique properties, including quantum confinement, surface plasmonic resonance, and large surface area, curvature, and surface roughness. When dispersed in a medium, NPs could aggregate into clusters or various lattices[1–3] with controlled inter-particle distance for potential applications, including nanoantennae, photonic switches, waveguides, sensors, biomarkers, and structural color.[4–9] There has been rising interest in directing colloidal particle assembly in liquid crystals (LCs), which are known for their anisotropic thermal, optical, electrical, and magnetic properties.[10] The particles can be trapped by the topological defects created *via* the orientational elasticity and surface anchoring of the surrounding LCs, leading to much richer assembled structures than those in an isotropic medium.[11–20] From a technological standpoint, the ability to tailor the topological defects will offer new tools to design, fabricate, and dynamically tune the advanced materials and devices. While a few groups have begun to assemble quantum dots or metallic NPs in nematic LCs,[21,22] most of the studies reported in the literature focus on micron-sized particles dispersed in nematic LCs, where elasticity dominates over thermal fluctuations. Compared with nematic LCs, which have only orientational order wherein molecules self-align along their common long axis, smectic LCs have both orientational and translational long-range ordering, and thus can arrange into layers or planes with the long molecular axis parallel to the layer normal. Previously, we and others have created a variety of complex arrays of focal conic domains (FCDs) from smectic-A (SmA) LCs assembled on topographically patterned substrates and interfaces, including one-dimensional (1D) channels,[23,24] holes,[25] micropillar arrays,[26,27] and colloids.[28] These defect domains arise from a balance of the elastic energy cost of layer bending and the anchoring energies on bounding surfaces, typically planar anchoring on the substrate and homeotropic anchoring (*i.e.*, in perpendicular orientation) at the LC/air interface.

It is of interest to exploit the defects arising from this competition between elasticity and surface anchoring to direct particle assembly within SmA LCs. Yoon *et al.* show that silica microparticles (diameter, 1 μm) are predominantly localized in

[a] *Department of Chemical and Biomolecular Engineering, University of Pennsylvania, Towne Building, 220 South 33rd Street, Philadelphia, PA 19104, USA. E-mail: shuyang@seas.upenn.edu; Tel: +1 215-898-9645*
[b] *Graduate School of Nanoscience and Technology, KAIST, 291 Daehak-ro, Yuseong-gu, Daejeon 305-701, Republic of Korea*
[c] *Department of Physics and Astronomy, University of Pennsylvania, 209 South 33rd Street, Philadelphia, PA 19104, USA*
[d] *Department of Materials Science and Engineering, University of Pennsylvania, 3231 Walnut Street, Philadelphia, PA 19104, USA*

† Electronic supplementary information (ESI) available. See DOI: 10.1039/c5sm01458a

‡ Current address: School of Engineering and Applied Sciences, Harvard University, 29 Oxford Street, Cambridge, MA 02138, USA.

the vertical line defect of a toric focal conic domain (TFCD) in a semi-fluorinated SmA LC (F-LC).[23] One possible explanation is the tangential surface anchoring of SmA LCs at the particle surface. Pratibha *et al.* find that when gold NPs (diameter, ~7 nm) with planar anchoring are dispersed in SmA LC, 4-*n*-octyl 4′-cyanobiphenyl (8CB), the layer structure and elasticity of SmA LC stabilize NPs at the smectic phase.[29] NPs can perturb the flat smectic layers at distances much larger than the particle size, forming bumps. However, the motion of NPs across the layers is hindered. This raises the intriguing questions of how, and to what degree, do NPs move within LC layers? What are the effects of surface anchoring and particle size on the trapping or motion of NPs within SmA layers? Will NPs distort or even topologically alter the assembly of SmA layers?

Here, we report synergistic assembly between F-LC and fluorosilane functionalized silica (F-SiO_2) NPs, which have high affinity to each other due to the semi-fluorinated chain ends and thus planar surface anchoring. Both scanning electron microscope (SEM) images and grazing incidence X-ray diffraction (GIXD) patterns show that when cooled from the isotropic phase to SmA phase F-SiO_2 NPs (100–500 nm in diameter) migrate as a group within seconds from the bottom to the top of the LC film through the central cusp defects of TFCDs. The TFCDs are formed by the SmA LCs to relax competition between planar anchoring at the lower interface, where NPs sit to cover the substrate, and homeotropic anchoring at the LC/air interface. When the migrated NPs form a monolayer that completely covers the LC/air interface, the surface anchoring of SmA LC at the top interface transforms from homeotropic to planar, resulting in vertically aligned layers between the top and bottom planar surfaces. In comparison, no co-assembly is observed between LCs and pristine SiO_2 NPs, on whose surface LC has homeotropic anchoring. SEM images reveal three different regimes depending on the degree of the elastic force and surface energy experienced by the particles of different sizes, including (i) a weak-anchoring regime when F-SiO_2 NP diameter < 500 nm, where NPs do not cause appreciable layer curvature and NP migration is driven by surface energy; (ii) a critical region at F-SiO_2 NP diameter ≈ 500 nm, and (iii) when F-SiO_2 particle diameter > 500 nm, that is comparable to or larger than the TFCD domain size, strong distortions occur in the smectic layers. The particle is found suspended at the TFCD defect core, much like the observation by Yoon *et al.*[23]

Experimental

Materials

The semi-fluorinated smectic liquid crystal (F-LC), (4′-(5,5,6,6,7,7,8,8,9,9,10,10,11,-11,12,12,12-heptadecaflu-orodo-decyloxy)-biphenyl-4-carboxylic acid ethyl ester, see the chemical structure in Fig. 1a) were synthesized according to our prior report.[26] The F-SiO_2 NPs of different diameters were prepared from silica NPs (d = 20 ± 3 nm, 100 ± 5 nm, 500 ± 5 nm, 1 ± 0.05 μm and 5 ± 0.35 μm, 30 wt% in isopropanol from Nissan Chemicals) with (heptadecafluoro-1,1,2,2-tetrahydrodecyl) dimethylchlorosilane (HDFTHD) (99%) (Gelest, Inc.) following the literature.[30]

Sample preparations

F-SiO_2 NPs were dispersed in the fluorinated solvent, Novec 7300 (3 M) at 2.5 wt%, followed by a 30 min sonication. F-SiO_2 NP solution was then spin coated onto a clean 2 × 2 cm^2 silicon wafer (2000 rpm for 30 s) for 3 times to obtain multilayered NPs completely covered on Si wafer before drop casting 200 μL F-LC solution, where F-LCs were well mixed with Novec 7300 at 10% (w/v) with 30 min sonication. The mixture on the substrate was heated on a Mettler FP82 and FP90 thermo-system hot stage to the isotropic phase at 200 °C for 5 min, cooled down to smectic phase at 114 °C at 5 °C min^{-1}, and subsequently quenched to room temperature by removing the sample from the hot stage (Fig. 1b). To observe intermediate states of the hybrid structures during thermal transition, the heated samples were removed from the hot stage at a specific temperature and immediately dipped into liquid nitrogen to solidify the structures. As seen in Fig. 2, when NP concentration was too low (≤1 wt%), we did not see NPs on LC film top. When NP concentration was high (≥ ~10 wt%), it was difficult to see the intermediate states. So we kept the NP concentration at ~2. 5 wt% in the experiments performed here, where we could clearly NP migration through the TFCD dimple.

Characterizations

All samples were imaged by SEM on a FEI Strata DB235 focused ion beam system at 5 kV. The reorganization process of LC and particles was recorded and captured by Olympus BX61 motorized optical microscope equipped with crossed polarizers using CellSens software.

Grazing incident X-ray diffraction (GIXD) experiments were carried out at the 9A beam line of the Pohang Light Source (PLS-II), Korea, following the same setup reported in literature.[31] The size of the focused beam was ~70 (V) × 450 (H) μm^2, and the energy was 11.08 keV. The sample-to-detector distance was fixed at 238 mm in order to investigate the wide-angle diffraction pattern profile. The diffraction patterns were typically recorded using a two-dimensional charge-coupled device (2D CCD) detector (Rayonix SX165, USA).

Results and discussion

To study the interactions between NPs and SmA LCs at a dynamic interface, and thus their respective self-assembly structures, we designed a system comprising spherical silica NPs treated with fluorosilane chemistry and rigid rod-like biphenyl LC molecules with semi-fluorinated chains (F-LC). The F-LC undergoes phase transitions from isotropic phase to SmA phase ($T_{SmA,I}$), the SmX phase, and crystalline state (T_C) at 185 °C, 111 °C, and 50 °C, respectively, during cooling.[26] Compared to the commonly used thermotropic SmA LCs, 8CB (T_C = 21.5 °C, $T_{SmA,N}$ = 33.5 °C, $T_{N,I}$ = 40.5 °C), the F-LC can be quenched quickly from SmA phase to room temperature while

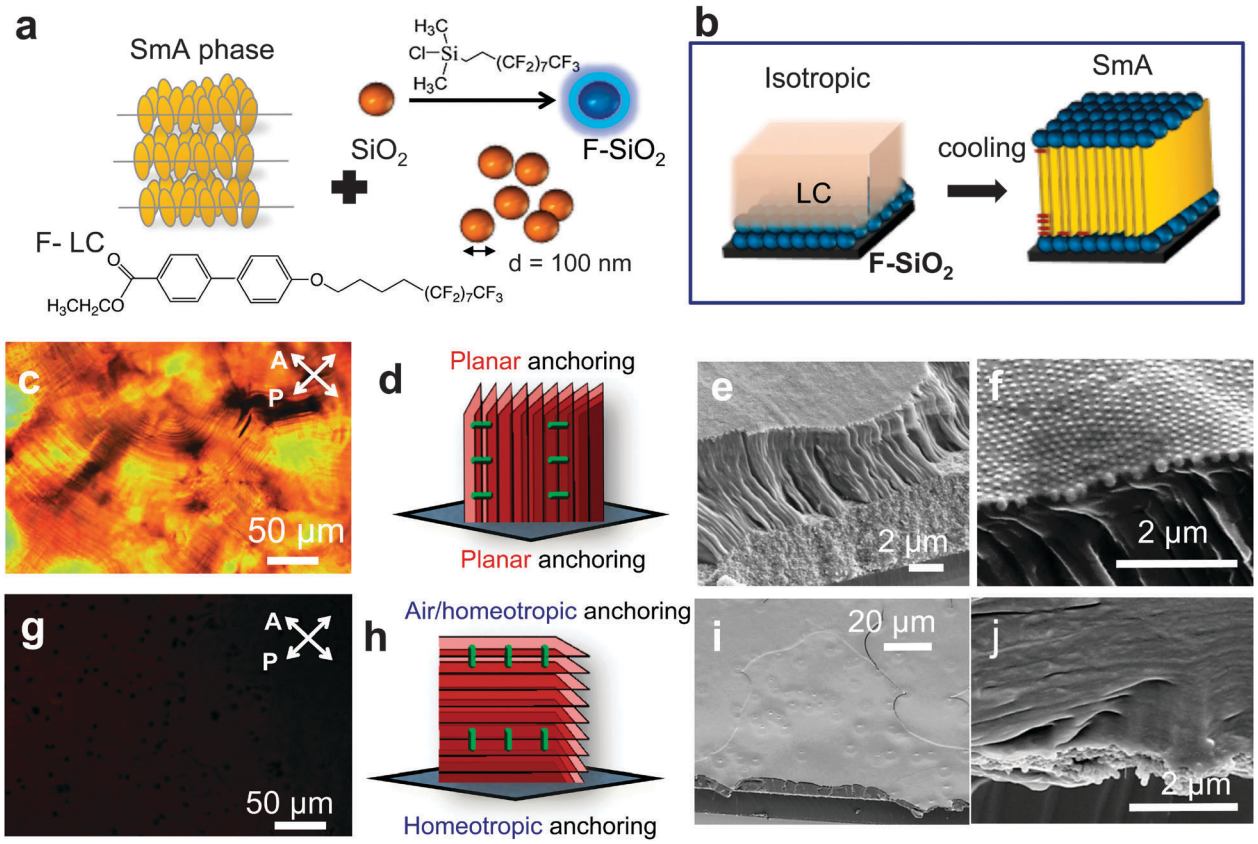

Fig. 1 Assembly of silica nanoparticles (diameter 100 nm) in SmA LC. (a) Illustrations of the chemical structure of F-LC, the ground state structure of the smectic-A phase, where the yellow rod represents the LC molecule, and synthesis of F-SiO_2 NP. (b) Schematic illustration of the initial and final configurations of the hybrid system when cooling from isotropic phase to smectic phase. (c–f) Characterization of the hybrid structure consisting of F-LC and 100 nm F-SiO_2 NPs. (c) POM image of the top of the film. (d) Illustration of a possible LC molecular configuration with planar anchoring both on top and at the bottom. (e and f) SEM images of the cross-sectional view of the hybrid film. (f) Zoom-in image of (e). (g–j) Characterization of the hybrid structures consisting of F-LC and 100 nm pristine SiO_2 NPs. (g) POM image of the top of the film. (h) Illustration of a possible LC molecular configuration with homeotropic anchoring on top and at the bottom. (i and j) SEM images of the top-view (i) and cross-sectional view (j) of the hybrid film. (j) F-LC layers sitting on top of the SiO_2 NPs cast on the substrate.

preserving the original LC structure. The quenched structure can be conveniently characterized at room temperature using standard imaging techniques, including SEM and atomic force microscopy (AFM)[26,27] to investigate the LC assembly behaviors quenched at different temperatures.

Silica NPs were selected as a model system for the mobile phase to probe elasticity and surface anchoring effects at the interface. Silica NPs of uniform and variable size ranging from tens of nanometers to microns are readily available commercially or they can be synthesized by Stöber reactions.[32] Their

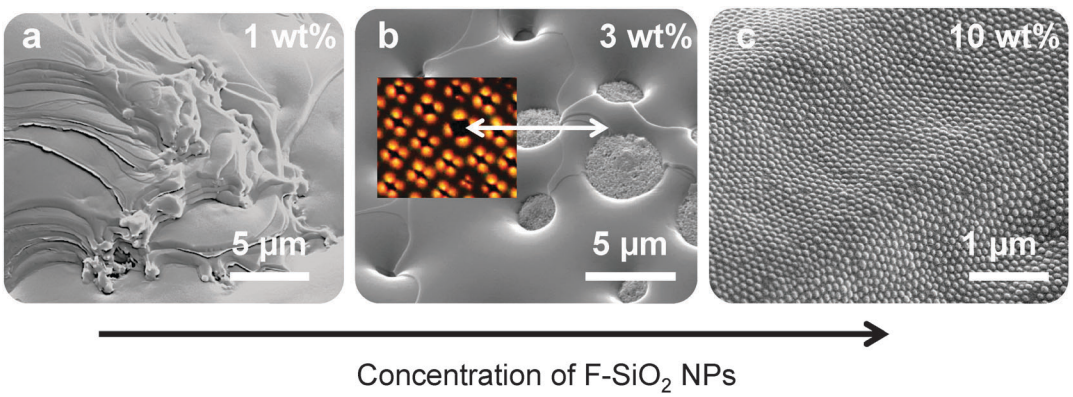

Fig. 2 SEM images of F-SO_2 NP/F-LC films prepared from different NP concentrations, and quenched from 114 °C. (a) 1 wt%. (b) 3 wt%. (c) 10 wt%. Inset in (b) is the POM image of the film, showing TFCD textures.

surface anchoring can also be fine-tuned *via* silane chemistry. In the design of a mobile interface between NPs and LCs, it is important that the surface chemistry of the particles should impart high affinity with the LCs to reduce NP aggregation, and thus enhance NP dispersion/motion in LC layers. Previously, we have synthesized F-SiO_2 NPs for preparation of transparent, superhydrophobic surfaces.[30] When dispersed in F-LC, which had similar semi-fluorinated groups, F-SiO_2 NPs show high compatibility with F-LC without much aggregation.

For the study here, it is also important that the NPs have sufficiently high mobility in F-LC such that the system can freely minimize its energy over both NP locations and smectic layer distortions, the latter induced by surface anchoring of the LC director at the NP surfaces. For comparison, we dispersed pristine silica particles with an oxide surface (denoted as SiO_2 NPs) in F-LC and studied their assembly structures within F-LC. To obtain qualitative information about the anchoring condition and the mobility of two types of NPs in F-LCs, we prepared NPs with diameter of 100 nm and examined their assembly behaviors in F-LC. The 100 nm NPs can be conveniently observed by SEM, yet are small enough for applications such as nanophotonics. The NP concentration was fine-tuned to make sure a complete coverage of the NPs on the flat substrate by spin coating. Since our aim is to study NP/LC interfaces and how the two materials direct the assembly of each other, it is essential to eliminate the substrate's interfacial effects on the F-LC.

After coating multilayered F-SiO_2 NPs on the Si wafer, F-LC was then cast on top at a temperature above the isotropic phase, followed by cooling to smectic phase and subsequently quenched to room temperature (see Fig. 1b). Polarized optical microscopy (POM) and SEM were used to monitor the structures of the composite at different temperatures. Bright fan-like textures in Fig. 1c were observed on the F-SiO_2 NPs/F-LC sample under the crossed polarizers. These fan-like textures changed local brightness with the rotating polarizers, which is characteristic of a birefringent SmA phase with focal conics, where lamellae of SmA LCs form a concentric roll when confined in a cell with planar anchoring surfaces.[33] The POM images suggested that domains of vertically aligned smectic layers constituted the hybrid F-SiO_2 NPs/F-LC structures, where the average field director lay parallel to the planes of the air/LC and LC/substrate interfaces, respectively (see schematic in Fig. 1d). This is only possible if there is planar alignment of the LC director at the upper interface. If the upper surface is air, which has strong homeotropic anchoring of F-LC and many other LC systems, TFCDs will form.[26,34] A closer look of the cross-sectional SEM images (Fig. 1e and f) revealed that indeed a monolayer of 100 nm F-SiO_2 NPs was arranged in a quasi-hexagonal array (interparticle spacing, $\sim$22 nm) on top of the aligned F-LC layers, replacing the air as illustrated in Fig. 1b. Clearly, F-LC has strong planar anchoring on the surface of fluorosilane modified F-SiO_2 NPs as expected. As a result, F-SiO_2 NPs should have high mobility in F-LCs. We note that the F-LC layers are not perfectly vertically aligned when the SmA LC layers are at the boundary between a NP-covered region and a NP-depleted region. Detailed explanation and schematic can be found in ref. 28.

In contrast, the pristine SiO_2 NPs/F-LC sample appeared dark under the crossed polarizers in any orientation (see Fig. 1g). The result suggested that the director field averaged over the film thickness ($\sim$10 μm) was normal to the plane of the film interface, that is, F-LC had homeotropic anchoring to the surface of pristine SiO_2 NPs (see schematic in Fig. 1h). In agreement with POM analysis, SEM images showed that the 100 nm SiO_2 NPs remained at the bottom of the horizontally aligned F-LC layers, with no appearance of NPs at the air/F-LC interface (see top-view, Fig. 1i, and cross-sectional-view, Fig. 1j). We note that the shallow dot-like defects seen in Fig. 1i should not be TFCDs since their birefringence is not noticeable under POM (see Fig. 1g). They could be random defects generated from the originally bumpy surface of pristine NPs spin cast onto the substrate. Since F-SiO_2 NPs showed high dispersion and mobility in F-LCs, we concluded that the clear phase separation between the pristine SiO_2 NPs and F-LC should be attributed to the dissimilar chemistry/surface energy between the hydrophobic F-LC molecules and the hydrophilic oxide surface of SiO_2 NPs. In short, the SiO_2 NPs were immobile in F-LC in all LC phases.

Rapid transitions between states in the F-SiO_2 NPs/F-LC system are imperative to realize the aforementioned behaviors, which involve the conveyance of the particles directed by F-LC, re-organizations of F-LC dictated by the organized F-SiO_2 NPs, and more importantly, the synergy between the interactions of F-SiO_2 NPs and F-LC molecules. Using optical microscopy, we performed *in situ* observation of the hybrid film during cooling from the isotropic phase to the SmA phase. As seen in Video S1 (ESI†), the POM textures revealed a gradual transformation of the hybrid system from TFCDs to fan textures with multiple intermediate states when cooled from the isotropic phase (200 °C) to SmA phase (114 °C). The texture appearing under the crossed polarizers rapidly evolved from complete darkness to 2D arrays of TFCDs, to a mixture of TFCDs and growing fan textures with vertically aligned layer structure within a few seconds, and eventually completely transitioned to microscopic fan textures. In the SmA phase, the coverage of the fan textures persisted over the entire film, suggesting a stable form of the hybrid system, which remained unchanged over an hour-long period when holding at the smectic phase, 114 °C, with only small variations possibly due to the temperature fluctuation of the hot stage.

In order to verify this layering configuration change at the layer/molecular level during the phase transition from isotropic to SmA phase, we carried out the grazing incidence X-ray diffraction (GIXD) experiments using the same setup reported earlier.[31] The scattering intensity profile, $I(q)$, gives orientation information and d-spacing on both interlayer (small-angle region) and intralayer molecular arrangement (wide-angle region). Here, q is the scattering factor, $q = \frac{4\pi \sin(\theta/2)}{\lambda}$, where λ is the wavelength and θ is the scattering angle. Two samples were prepared from F-SiO_2 NP/F-LC but quenched at different

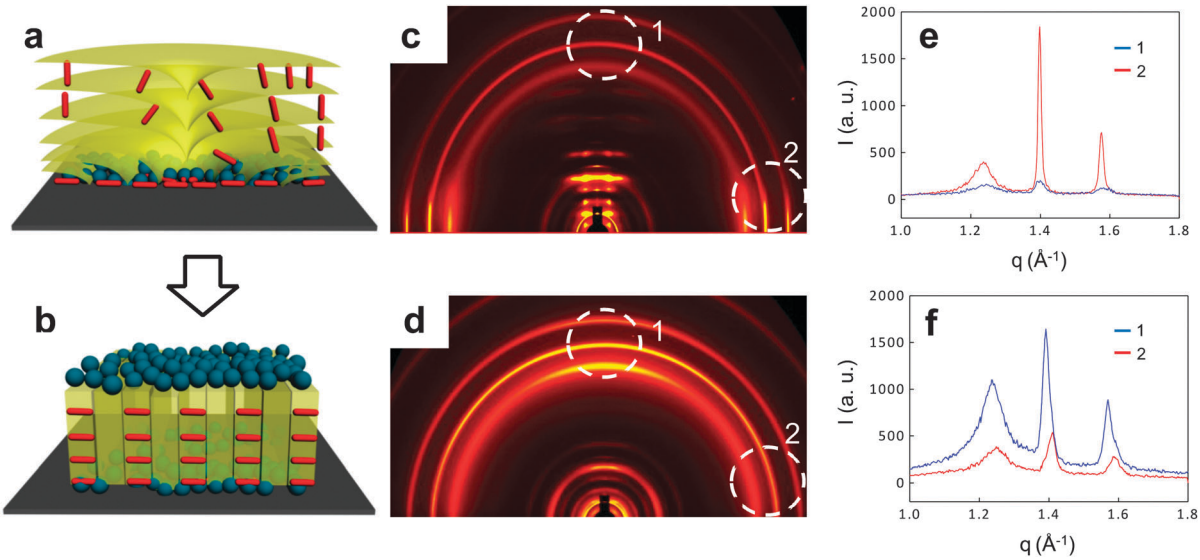

Fig. 3 SmA layer arrangement and the corresponding molecular ordering of the hybrid F-LC/F-SiO2 NP structures. (a and b) Schematic illustrations of two samples prepared at different conditions. Red rods represent LC molecules and green spheres are for F-SiO_2 NPs. (a) TFCD and F-SiO_2 NPs on the bottom substrate. (b) Vertically aligned LC layers and migrated NPs on top of the LC film. (c and d) 2D GIXD patterns of samples prepared at different conditions, showing the orientation of layers and the molecules. (c) Quenched at isotropic temperature, 200 °C. (d) Quenched at smectic phase, 114 °C. (e and f) Corresponding 1D GIXD diffraction intensity *I vs.* the scattering angle [$q \sim \sin(\theta/2)$] in the wide-angle region with vertical and horizontal line-cut, showing out-of-plane (planar anchoring, 1; blue) and in-plane (homeotropic anchoring, 2; red) molecular ordering.

temperatures. One was directly quenched from T_{iso} = 200 °C to room temperature; the particles were found remaining on the substrate with the F-LC forming TFCDs (Fig. 3a, c and e). The second sample was quenched from the smectic phase, T_{SmA} = 114 °C after cooling from T_{iso}. The particles were found popping-up to the top of the LC film, replacing the air at the top interface, thus, inducing vertical layer arrangements (Fig. 3b, d and f), in agreement with SEM results. Fig. 3c shows the typical 2D diffraction pattern of a TFCD;[23] tangential alignment of layers is formed in the small-angle region while the horizontal lines are found in the wide-angle region. On the contrary, Fig. 3d shows planar alignment of LC molecules in the wide-angle region, resulting from vertically aligned layers as shown in Fig. 3b.[35] The corresponding diffraction intensity profile in the wide-angle region confirms this dramatic orientation change quantitatively (Fig. 3e and f); vertical (1; blue line) and horizontal (2; red line) line-cut 1D graphs show planar and homeotropic arrangements of the aligned molecules at each condition, respectively. For example, the very strong and sharp intensity of red line that represents the strong homeotropically aligned molecules (Fig. 3e) is much weakened when the molecules are aligned parallel to substrate (Fig. 3f). Thus, the GIXD results confirmed that sample quenching temperature was critical, suggesting elasticity of the smectic phase played a role in NP migration. In turn, the assembly location of F-SiO_2 particles could globally induce very different orientations of the F-LC layering structures.

The route that F-SiO_2 NPs traveled through the F-LC layers from the bottom of the substrate to the top F-LC/air interface may afford additional information regarding intermediate states and the phase transition of the hybrid structure. Naïvely, we may picture the F-SiO_2 NPs on the substrate travelling upward in a straight-line manner, which might be the case in LCs without a quasi-2D translational order. However, since the formation of FCDs occurred during the initial state of cooling from the isotropic phase, the NPs are presumably attracted or trapped in the high-energy region at the center of the FCDs to minimize the energy penalty associated with the curvature and elastic disruptions in the low-energy region of the lamellar structure.

Again, we resorted to SEM to image F-SiO_2 NP/F-LC films at different intermediate states (see Fig. 4a–d) quenched at temperatures ranging from 160–120 °C using liquid nitrogen. Fig. 4a shows the as-cast F-SiO_2 NP assembly on a substrate, which is nearly close-packed. When the sample was quenched at 160 °C, the F-LC first formed an array of TFCDs with particles drifting up toward the top interface along the defect lines (Fig. 4b). This indicated that the TFCDs could form at the virtually instant cooling rate, while the NPs traveled through the ~10 μm thick film to the top interface within the time frame of a few seconds. Fig. 4c shows a close-up view of NPs traveled along the dimple of a TFCD at 140 °C. Concentric rings near the dimple sites are clearly seen as a result of sublimation and recondensation of the SmA LCs.[36–38] At 120 °C, the top surface of the film was nearly completely covered by the NPs (Fig. 4d). The result also suggested that NPs at the bottom of the substrate did not move individually but rather migrated as a group through the disclination line in the center of TFCD (see a schematic illustration in Fig. 4e). These images are consistent with our *in situ* observation shown in Video S1 (ESI†).

Here, the reorganization of the mobile NPs from the bottom of F-LC film to the top interface and the concurrent reconstruction of

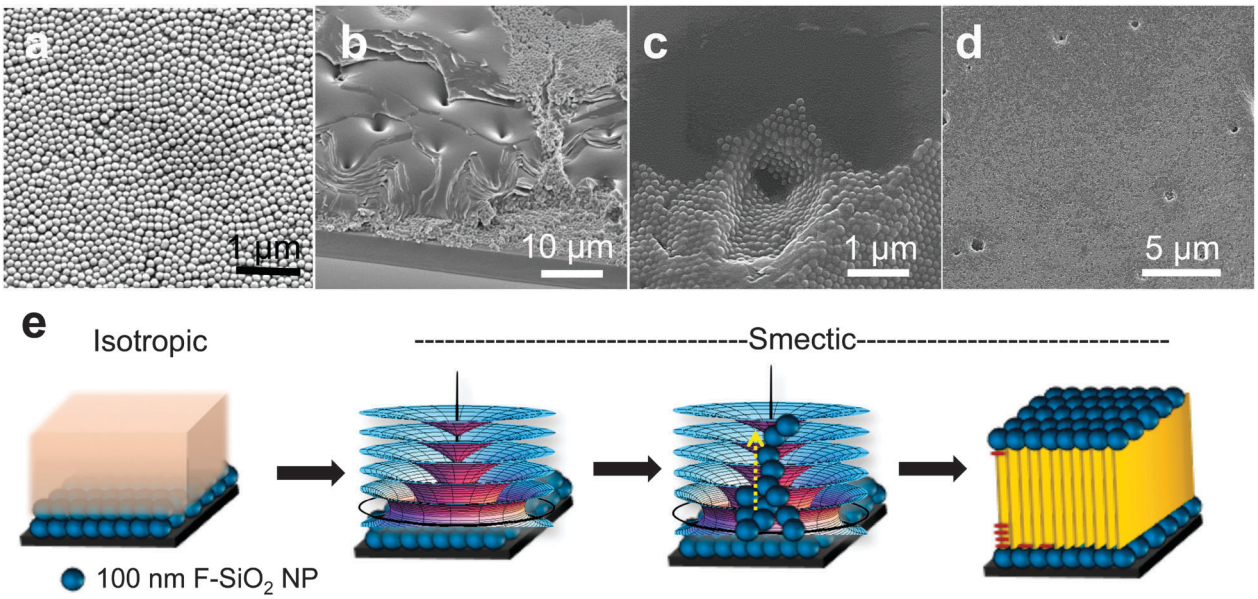

Fig. 4 F-SiO_2 NP (100 nm in diameter)/F-LC hybrid film at different states when quickly quenched at various temperatures. (a–c) SEM images. (a) As-cast F-SiO_2 NP film on the substrate. (b–d) Hybrid films at (b) 160 °C, (c) 140 °C, and (d) 120 °C. (c) Close-up view at a TFCD dimple. (e) Schematic illustrations of the structural transformation of the hybrid film during cooling from isotropic phase to smectic phase.

the LC director structure implied a synergistic effect in an anisotropic fluid. As mentioned earlier, appropriate surface chemistry of the NPs plays a key role that enables the mobility of the NPs in the LC media. The specific path of how the NPs traveled suggested that the movement of the NPs was predominantly driven by the elastic force of the smectic LC expelling the NP inclusions toward defect lines and guiding them to the free surface, where they remain trapped owing to capillary trapping energies.

To further develop the potential of F-SiO_2 NP/F-LC system toward various applications, we performed the same experiments from F-SiO_2 NPs of different sizes, including 10 nm, 20 nm, 100 nm, 500 nm, 1 μm and 5 μm in diameter. The results of this set of experiments revealed two important aspects of the system. First, the organization of the F-SiO_2 NP/F-LC system was particle size-dependent, leading to diverse hybrid structures (see Fig. 5a–h). Second, based on the degree of the elastic force and surface energy experienced by the particles in the system, the arrangement of F-LC and F-SiO_2 can be classified into three different regimes: (i) a weak-anchoring regime when F-SiO_2 NP diameter $<$ 500 nm, where NPs do not cause appreciable layer curvature and NP migration is

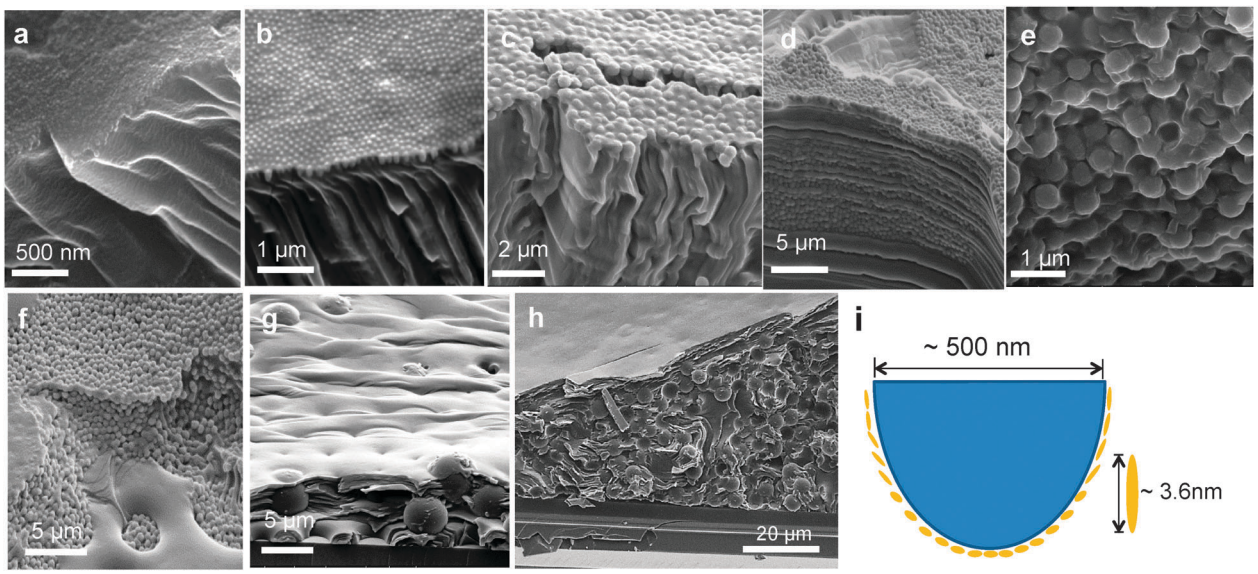

Fig. 5 Effect of particle size on the assembly of F-SiO_2 particles in F-LC. (a–h) SEM images of the final hybrid structures with various F-SiO_2 particle diameters: (a) 20 nm, (b) 100 nm, (c–f) 500 nm at different regions of the film, (g and h) 5 μm. (e) A close-up view of 500 nm particles in different layers as seen in (d). (i) Schematic illustration of planar anchoring LC molecules on a 500 nm particle surface.

driven by surface energy; (ii) a critical region at F-SiO_2 NP diameter $\approx$ 500 nm, and (iii) large-NP behavior for F-SiO_2 particle diameter $>$ 500 nm, where smectic layers strongly curve in response to particle surface energy, and the particles remain suspended in the bulk.

Fig. 5a and b revealed the similar formation of vertically aligned smectic layer structures sandwiched between layers of F-SiO_2 NPs with diameter of 20 nm and 100 nm, respectively. When the F-SiO_2 NP diameter was increased to 500 nm, the final state comprised a mixture of two different configurations: the vertically aligned smectic layer structure (Fig. 5c) and primarily a 2D packing of NPs fused in each layer of horizontally aligned smectic structure (see Fig. 5d–f). The presence of two structures clearly indicated that the system had reached the critical point, above which the total free energy of the vertically aligned smectic layer structure was no longer at the minimum. The data could be rationalized by a simple analysis on molecular structure. As seen from the schematic illustration of the uniform configuration of vertically aligned smectic layer structure (Fig. 4e), the surface at the top film interface composed of 2D packed F-SiO_2 NPs would favor parallel alignment of F-LC molecules that are $\sim$3.6 nm long. However, when the particle size is increased to 500 nm, the large surface contour and its curvature inevitably distort the planar anchoring of LCs on NPs, thus, the packing of vertically aligned smectic layers (over 200) on the NP surface (see schematic in Fig. 5i), and impose a huge energy penalty for the molecules tilted out of the horizontal direction. The condition with 500 nm F-SiO_2 simply does not satisfy the uniform configuration of the vertically aligned smectic layer since it demands the average orientation of F-LC molecules to be planar throughout the film.

When particle size is small and the surface anchoring is weak, the NP does not alter the smectic layers around it, so the elastic force should arise only from the gradient in the elastic energy density of the TFCD itself (the elastic energy cost of the small region that the NP replaces). However, this elastic force would push the particle downward. The smectic elastic energy density $f_{el} \sim (1/R_1 + 1/R_2)^2$ increases as the layers' principal radii of curvature R_1, R_2 decrease. In a TFCD, R_1, R_2 are the distance from the circular defect and the central line defect, respectively.[26,39] Therefore, near the central line defect, the elastic energy density is larger closer to the bottom where R_1 is smaller. So the upward lifting force must come from the NP surface energy. Yoon *et al.* have estimated the surface anchoring energy cost as a function of particle height z in the central line defect, in the case when the particle radius R is much smaller than the radius a of the TFCD. They derive the vertical force for the vertical line defect to push the particle upwards as[23]

$$f_{anch} = (8/3)\pi R^2(\sigma_\perp - \sigma_\parallel)\left(\frac{\delta}{a}\frac{1}{(1+\delta^2)^2}\right) \quad (1)$$

where $\sigma_\parallel$ and $\sigma_\perp$ are the surface energy densities for molecules oriented in parallel and perpendicular to the substrate, respectively, and $\delta = z/a$. A rough dimensional analysis suggests that the crossover length scale between weak and strong anchoring (compared to elasticity) should occur at a size, $R \sim K/(\sigma_\perp - \sigma_\parallel)$, where K is the curvature elastic constant of SmA, $\sim 5 \times 10^{-11}$ N.[26] Since the crossover particle size we observed in experiments was 500 nm, $(\sigma_\perp - \sigma_\parallel)$ was estimated $\approx 10^{-4}$ J m^{-2}. For R = 50 nm, a = 2 μm, and assuming δ = 1, f_{anch} is 500 times larger than the gravitational force, $f_g = (4/3)\pi R^3 \rho g \sim 5 \times 10^{-6}$ pN, where $\rho \sim 10^3$ kg m^{-3}, is the difference in densities of a silica particle and a liquid crystal, and g = 9.8 ms^{-2} is the acceleration of gravity. When particle size is small, the surface anchoring energy could power particles upward to the air/LC interface along the disclination line, overcoming the elastic energy of a TFCD, and the gravitational force is negligible. We note that here the estimation of the surface anchoring energy is oversimplified, since that in eqn (1) is derived for a single particle located in the center of a TFCD. In our experiment, a group of NPs migrate along the defect line of a TFCD dimple. More detailed theory will be needed to address this, but is beyond the scope here.

When the particle becomes bigger (*e.g.* $>$500 nm), it causes strong distortions in the smectic layers. Blanc and Kleman[39] have calculated the elastic energy of a SmA LC containing a spherical inclusion in the limit of infinitely strong anchoring. As a function of particle radius R, they calculate $F_{el} \sim R\ln(R/r_c)$, where r_c is a cutoff parameter, close to the smectic layer spacing, $\sim$3 nm. The layer configuration in this case contains a linear cusp defect emerging from opposite poles of the inclusion, similar to the central line defect of the TFCD. In our experiments, 5 μm diameter F-SiO_2 microparticles were found levitating in the smectic LC bulk, centered at a vertical defect line (see Fig. 5g and h). The smectic layer configuration in this case seems to be a combination of Blanc and Kleman's structure with a TFCD anchored at the substrate, producing TFCD-like dimples at the air interface, since the surface energies of all three surfaces are important. Consistent with the literature,[23,39] the straight line defect of the TFCD was the most preferable site for the microparticles due to the resulting beneficial overlap of the smectic layer deformations preferred by the various surfaces. In short, the TFCD array self-assembled by antagonistic boundary conditions (planar anchoring at the bottom and homeotropic anchoring on top) dictated the observed configuration of an array of trapped microparticles, which may in turn have helped to stabilize the TFCD array. Here, the discussion of the mechanism of levitating particles is mostly qualitative and has focused on the limits of weak and strong anchoring. It would be interesting in the future to quantitatively predict the smectic layer configurations arising from a balance of elasticity and finite surface anchoring of mobile particles.

Conclusion

We presented a dynamic hybrid system from SmA LC and F-SiO_2 NPs with planar anchoring surface, and demonstrated the synergistic assembly of the two materials. In the SmA phase, F-SiO_2 NPs sitting underneath LC films migrated

through the defect lines of SmA LC layers driven by planar anchoring surface energy and the LC elasticity. A monolayer of planar anchoring NPs was formed on top of the LC layers, replacing the homeotropic air interface, and in turn altering the assembly of SmA LCs from TFCD arrays into vertically aligned layers. We showed that surface chemistry and size of the particles played key roles in engineering the dynamic particle/LC interface and the resulting structures. The high affinity of fluorosilane treated F-SiO_2 NPs with semi-fluorinated F-LC promoted planar anchoring of the LC on NP surfaces and high mobility of NPs in LCs. The size of the particle should be smaller than the equivalence of $\sim$200 smectic layers (in this case, 500 nm in diameter) to obtain vertically aligned SmA layers. We investigated the mechanism of the synergistic assembly phenomenon as a means to fully explore the potential application of such hybrid materials systems. Our study revealed that when the particle size was small (diameter $<$ 500 nm), they drifted as a group in concert from the bottom of the LC film to the top interface along the defect line at the center of an FCD when transitioning from the isotropic phase to the smectic phase. The knowledge of the intermediate states of the NP/LC hybrid structures will provide valuable insights to assemble functional nanomaterials such as quantum dots (suggested by our preliminary results) and metallic NPs in an anisotropic medium and take advantage of their collective assembly behaviors.

Acknowledgements

This work was supported by the National Science Foundation (NSF) Materials Science and Engineering Center (MRSEC) Grant to the University of Pennsylvania, DMR-1120901, and the National Research Foundation (NRF) by the Korean Government (MSIP) (grant #, 2014M3C1A3052537). This work is also partially supported by a Simons Investigator grant from the Simons Foundation to R.D.K. D.A.B. was supported by NSF Grant DGE-1321851. The Nanoscale Characterization Facility (NCF) at Penn and the Laboratory for Research on the Structure of Matter (LRSM) are acknowledged for access to SEM. Experiments at the PLS-II were supported in part by MSIP and POSTECH.

References

1 M. E. Leunissen, A. van Blaaderen, A. D. Hollingsworth, M. T. Sullivan and P. M. Chaikin, *Proc. Natl. Acad. Sci. U. S. A.*, 2007, **104**, 2585.
2 Y. Min, M. Akbulut, K. Kristiansen, Y. Golan and J. Israelachvili, *Nat. Mater.*, 2008, **7**, 527.
3 D. V. Talapin, E. V. Shevchenko, M. I. Bodnarchuk, X. Ye, J. Chen and C. B. Murray, *Nature*, 2009, **461**, 964.
4 C. B. Murray, C. R. Kagan and M. G. Bawendi, *Science*, 1995, **270**, 1335.
5 A. Burns, H. Ow and U. Wiesner, *Chem. Soc. Rev.*, 2006, **35**, 1028.
6 F. Li, D. P. Josephson and A. Stein, *Angew. Chem., Int. Ed.*, 2011, **50**, 360.
7 H. Wang, D. W. Brandl, P. Nordlander and N. J. Halas, *Acc. Chem. Res.*, 2006, **40**, 53.
8 S. H. Kim, H. Hwang, C. H. Lim, J. W. Shim and S. M. Yang, *Adv. Funct. Mater.*, 2011, **21**, 1608.
9 S. H. Kim, J. W. Shim and S. M. Yang, *Angew. Chem., Int. Ed.*, 2011, **50**, 1171.
10 P. G. De Gennes and J. Prost, *The Physics of Liquid Crystals*, Clarendon Press, Oxford, 1993.
11 I. Muševi̇ and M. Škarabot, *Soft Matter*, 2008, **4**, 195.
12 I. Muševič, M. Škarabot, U. Tkalec, M. Ravnik and S. Žumer, *Science*, 2006, **313**, 954.
13 G. M. Koenig, I. H. Lin and N. L. Abbott, *Proc. Natl. Acad. Sci. U. S. A.*, 2010, **107**, 3998.
14 T. Ohzono and J.-I. Fukuda, *Nat. Commun.*, 2012, **3**, 701.
15 A. Martinez, M. Ravnik, B. Lucero, R. Visvanathan, S. Žumer and I. I. Smalyukh, *Nat. Mater.*, 2014, **13**, 258.
16 I. I. Smalyukh, Y. Lansac, N. A. Clark and R. P. Trivedi, *Nat. Mater.*, 2010, **9**, 139.
17 M. A. Gharbi, M. Nobili, M. In, G. Prevot, P. Galatola, J.-B. Fournier and C. Blanc, *Soft Matter*, 2011, **7**, 1467.
18 M. A. Gharbi, M. Cavallaro, G. Wu, D. A. Beller, R. D. Kamien, S. Yang and K. J. Stebe, *Liq. Cryst.*, 2013, **40**, 1619.
19 M. Cavallaro, M. A. Gharbi, D. A. Beller, S. Čopar, Z. Shi, T. Baumgart, S. Yang, R. D. Kamien and K. J. Stebe, *Proc. Natl. Acad. Sci. U. S. A.*, 2013, **110**, 18804.
20 M. Cavallaro, M. A. Gharbi, D. A. Beller, S. Copar, Z. Shi, R. D. Kamien, S. Yang, T. Baumgart and K. J. Stebe, *Soft Matter*, 2013, **9**, 9099.
21 A. L. Rodarte, R. J. Pandolfi, S. Ghosh and L. S. Hirst, *J. Mater. Chem. C*, 2013, **1**, 5527.
22 A. Abass, S. R.-K. Rodriguez, T. Ako, T. Aubert, M. Verschuuren, D. Van Thourhout, J. Beeckman, Z. Hens, J. Gómez Rivas and B. Maes, *Nano Lett.*, 2014, **14**, 5555.
23 D. K. Yoon, M. C. Choi, Y. H. Kim, M. W. Kim, O. D. Lavrentovich and H.-T. Jung, *Nat. Mater.*, 2007, **6**, 866.
24 Y. H. Kim, D. K. Yoon, M. C. Choi, H. S. Jeong, M. W. Kim, O. D. Lavrentovich and H.-T. Jung, *Langmuir*, 2009, **25**, 1685.
25 W. Guo, S. Herminghaus and C. Bahr, *Langmuir*, 2008, **24**, 8174.
26 A. Honglawan, D. A. Beller, M. Cavallaro, R. D. Kamien, K. J. Stebe and S. Yang, *Adv. Mater.*, 2011, **23**, 5519.
27 A. Honglawan, D. A. Beller, M. Cavallaro, R. D. Kamien, K. J. Stebe and S. Yang, *Proc. Natl. Acad. Sci. U. S. A.*, 2013, **110**, 34.
28 D. A. Beller, M. A. Gharbi, A. Honglawan, K. J. Stebe, S. Yang and R. D. Kamien, *Phys. Rev. X*, 2013, **3**, 041026.
29 R. Pratibha, W. Park and I. I. Smalyukh, *J. Appl. Phys.*, 2010, **107**, 063511.
30 L. Xu, R. G. Karunakaran, J. Guo and S. Yang, *ACS Appl. Mater. Interfaces*, 2012, **4**, 1118.
31 H. Kim, S. Lee, T. J. Shin, E. Korblova, D. M. Walba, N. A. Clark, S. B. Lee and D. K. Yoon, *Proc. Natl. Acad. Sci. U. S. A.*, 2014, **111**, 14342.

32 W. Stöber, A. Fink and E. Bohn, *J. Colloid Interface Sci.*, 1968, **26**, 62.
33 Y. H. Kim, D. K. Yoon, H. S. Jeong, J. H. Kim, E. K. Yoon and H.-T. Jung, *Adv. Funct. Mater.*, 2009, **19**, 3008.
34 J. P. Bramble, S. D. Evans, J. R. Henderson, T. J. Atherton and N. J. Smith, *Liq. Cryst.*, 2007, **34**, 1137.
35 D. K. Yoon, J. Yoon, Y. H. Kim, M. C. Choi, J. Kim, O. Sakata, S. Kimura, M. W. Kim, I. I. Smalyukh, N. A. Clark, M. Ree and H. T. Jung, *Phys. Rev. E: Stat., Nonlinear, Soft Matter Phys.*, 2010, **82**, 041705.
36 D. K. Yoon, Y. H. Kim, D. S. Kim, S. D. Oh, I. I. Smalyukh, N. A. Clark and H.-T. Jung, *Proc. Natl. Acad. Sci. U. S. A.*, 2013, **110**, 19263.
37 D. S. Kim, Y. J. Cha, H. Kim, M. H. Kim, Y. H. Kim and D. K. Yoon, *RSC Adv.*, 2014, **4**, 26946.
38 D. S. Kim, A. Honglawan, K. Kim, M. H. Kim, S. Jeong, S. Yang and D. K. Yoon, *J. Mater. Chem. C*, 2015, **3**, 4598.
39 C. Blanc and M. Kleman, *Eur. Phys. J. E: Soft Matter Biol. Phys.*, 2001, **4**, 241.